

Improvement of Optical Setup of the Novel 2D Single-Shot Comb-Based Interferometer for High-Resolution Measurement

Dinh Thai Bao¹, Truong Cong Tuan², Tatsutoshi Shioda^{1*}

¹Graduate School of Science and Engineering, Saitama University, Saitama, Japan

²School of Mechanical Engineering, Hanoi University of Science and Technology, Hanoi, Vietnam

*Email: tshioda@mail.saitama-u.ac.jp

Abstract

The novel 2D single-shot comb-based interferometer introduces a massive potential for inline inspection in the industrial chain. The system's advantages are based on a novel optical setup, which combines a new customized infrared pseudo comb light source with a reflected blaze grating acting as a spatial phase modulator. The optical comb source with multiple comb order introduces the system's fantastic ability to extend the measurement range far from the traditional interferometers. At the same time, the grating modulates the incident light into a 2D reference with a delaying optical path difference to provide a real-time profilometry and tomography ability. This research analyzes the optical design to optimize the specifications of the grating and optical imaging lens. Optimized optics specification improves the profilometry resolution up to the micrometer scale, which was considered impossible in the previous system. Additionally, using the unique infrared pseudo frequency sweeping laser as the comb source, the system minimizes the natural speckle-noise effect from the optics, which is the barrier of all typically visible measurement systems. The experiment was successfully conducted to calibrate the new specifications of the system, followed by the experiment measuring the only 1 μm displacement of the mirror to discover the profilometry resolution improvement. The system's ability to measure the scattering sample is also investigated by the experiment inspecting the profile of a Japanese 10-yen coin. The research proves the 2D single-shot comb-based interferometer is one of the most powerful optical devices for industrial inline inspection.

Keywords: Optical profilometry, optical frequency comb, spatial phase modulator, high-resolution.

1. Introduction

Surface profilometry and tomography are always in high demand within industrial applications. Over the decades, the interferometers [1] prove to be the most potential optical measurement method for profilometry and tomography. There were abundant methods invented to improve the interferometer's resolution, measurement speed, or stability. The time-domain interferometers [2,3] offer high precision measurement up to micrometer-scale resolution by extracting the optical path difference caused by the scanning of the reference mirror. However, the time-consuming and the vibration of mechanical movement are the gap in adapting high-speed measurement. The Fourier domain interferometers [4] overcome the vibration drawback of non-mechanical scanning mechanism using the spectrometer. The measurement speed is also improved significantly with a high-speed camera, although the Fourier transforms in data processing still consume a long time in the case of complex data. In addition, the recent generation of profilometry and tomography can be mentioned as optical frequency comb-based interferometer.

The first concept of applying optical frequency comb into profilometry [5] is based on sweeping the comb interval corresponding to the mirror scanning in the time-domain interferometer. The system successfully produces an optical frequency comb source with a frequency interval of up to gigahertz, which is suitable for measuring the millimeter-scale sample. In the second generation, the novel setup using a virtual image phase array [6] or liquid crystal Fabry Perrot [7] introduces a new method to produce the optical frequency comb with a more straightforward setup. The light from a typical continuous broadband light source such as white light or supercontinuum laser is line-focused into the output plane of the VIPA by a cylindrical lens. Due to the multiple reflections inside the VIPA, only the frequencies in a constant spacing are emitted, producing an optical comb source. The high number of comb orders corresponds to the highly flexible measurement range. The reflected grating acting as a spatial phase modulator (SPM) modulates the optical path of the output light from the comb source to the 2D depth camera producing a reference signal with different depths. Therefore, the system offers a series of advantages of 2D detection, single-shot capturing, and flexible long-range

measurement using high-order comb interference. The following development, called axial zoomable 2D single-shot comb interferometer [8], upgrades the unique zooming function that allows the system to cover a dual-scale measurement. The grating orders are manipulated to adjust the measurement range, leading to profilometry resolution changes. The fine-scale mode switches the total eight diffraction orders of the SPM to adjust the measurement range flexibly from 200 μm to 1.2 mm while the coarse-scale mode enlarges the measurement range up to tens of millimeters. Despite considerable advantages, the second generation of 2D single-shot comb-based interferometer is still suffered from measuring the scattering sample where most of the reflected light is lost. Energy loss is the common problem of all the traditional optical frequency comb produced by setting the etalon after the typical light source. To solve the problem, the recent research on discrete frequency sweep laser [9] introduces a setup of etalon inside the cavity to compensate for the energy lost by the etalon. It results in the concentration of the lasing energy into each comb tooth to improve the comb energy significantly. Moreover, the unique setup allows the system to easily manipulate the sweeping repetition rate to overcome the vibration frequency of 1kHz in general industrial inspection. The system becomes high power and anti-vibration.

The performance of the 2D single-shot comb-based interferometer can be even much better with optical design optimization. This research deeply analyses the optical configuration to optimize the optics component specifications. The relationship between the grating groove spacing and the lens resolution is investigated to introduce a high-resolution measurement system. The system

successfully detects the mirror displacement of only 1 μm that the previous setup has not performed. The experimental results prove the system's feasibility in obtaining very high precision with potentially reaching a sub-micrometer resolution. Another experiment measuring a Japanese 10-yen coin is conducted to verify the system's ability to inspect the scattering samples. The research combines the advantages of the previous generations of the 2D single-shot comb-based interferometer to provide a powerful inspection tool with high-speed detection, long-range measurement, scattering minimization, and high resolution.

2. Operation Principle of 2D Single-Shot Comb-Based Interferometer

2.1. Configuration of 2D Single-Shot Comb-Based Interferometer

Fig. 1 shows the configuration of the 2D single-shot comb-based interferometer. The light source is a customized discrete frequency swept laser consisting of a spontaneous seed laser, a lasing medium, and a frequency tuning part. The output beam from the light source is a pseudo optical frequency comb, which emits infrared broadband light. Due to the natural characteristic of long wavelength, the light source minimizes the scattering effect when propagating the light beam to the optical components of the system. The beam expander expands the collimated light source before transferring the beam to the Michelson interferometer module, consisting of a unique grating arm and a sample arm. By setting up a reflected grating in the reference arm following the Littrow configuration, the grating acts as a spatial phase modulator to modulate the optical path of the incident beam in a 2D direction.

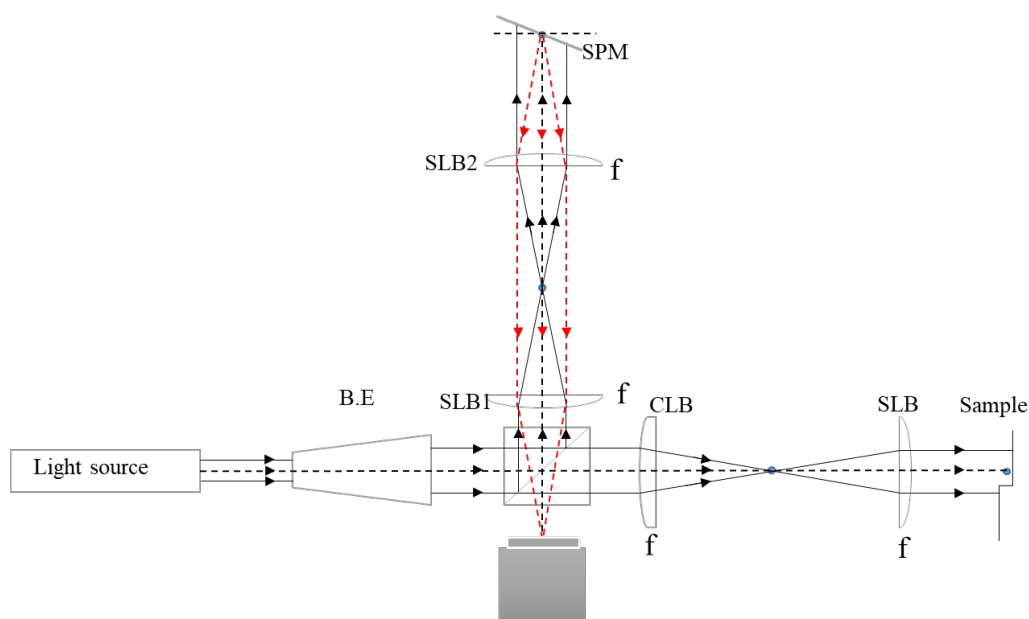


Fig. 1. Configuration of the 2D single-shot comb-based interferometer

The sample arm consists of a cylindrical lens, which converts the collimated incident beam into a horizontal line-focused beam before the spherical lens transforms the light into a sharp vertical line focusing onto the measured sample. The line profile of the sample is reflected through the lens system into the CCD camera to interfere with the reflected beam from the grating reference. Due to the spatial modulation of the grating, the delaying reference can interfere with reflection from the sample arm immediately to show the 2D profile of the measured sample in the real-time mode of the camera. The incline angle of the grating and the size of the light beam decide the single-shot measurement range, as in (1).

$$\Delta z = D \times \tan \alpha \quad (1)$$

where Δz is the measurement range, D is the diameter of the incident beam, and α is the diffraction angle from the grating. The 4f imaging lens system helps to remove the propagating aberration. Additionally, because the reflection efficiency of two interference arms is different, the beam splitter ratio is a factor in balancing the reflection intensity, enhancing the interference fringe contrast.

The detail of the effect of grating and the lens specification is described in the following section.

2.2. Operation Principle of Grating in Littrow Configuration

In the proposed 2D single-shot interferometer, a reflective grating acts as the spatial phase modulator configured in the Littrow configuration as Fig. 2. The grating equation in the case of the coincident incident beam and diffraction beam axis can be written in (2).

$$D \times \sin \theta = m \lambda. \quad (2)$$

where d is groove spacing, θ is blaze angle, m is diffraction order, and λ is blaze wavelength.

Due to the specular reflection in the Littrow configuration, the adjacent facets on the grating profile reflect the light with the delaying optical path. Therefore, the proposed system introduces the significant advantages of a 2D single-shot detection, which is equivalent to a whole scanning process of multiple steps in a traditional vertical scanning interferometer. The groove spacing implies the width of a grating facet which affects to diffraction efficiency of the grating. The discrete distance between the adjacent facets is called the blaze height (h), which can be computed geometrically by equation (3).

$$H = d \times \sin \theta. \quad (3)$$

Equation (3) shows the dependence of blaze height (h) upon the blaze angle of the spatial phase modulator. The measurement range can be adjusted by controlling the blaze angle. However, the size of the discrete blaze height also brings the concern about the discrete gap in the reference signal. In this case, the

interference signal will be ambiguous when measuring the profile more minor than the blaze height (h), which becomes the resolution limitation of the system in profilometry.

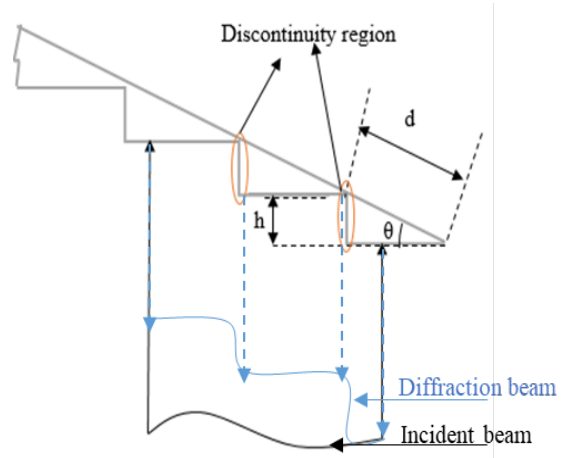


Fig. 2. Grating diffraction output in Littrow configuration.

The following section shows the effect of combing different grating specifications with the imaging lens, which should be matched to optimize the system resolution. Then, the experiment with the selected optical component is conducted to show the system's ability to measure high-resolution displacement.

3. Experimental Setup

3.1. Optimization of Axial Resolution by Selecting the Suitable Grating and Imaging Lens.

An experimental setup of the 2D single-shot comb-based interferometer is conducted with different grating specifications to show the relationship between lens resolution and grating specification. The first experiment uses a blazed grating of 300 lpm, which introduces a groove spacing (d) of 3.33 μm , while the second experiment uses an echelle grating of 79 lpm for the groove spacing of 12.65 μm . A spherical imaging lens with a focal length of 35 mm is employed right before the grating to map the grating diffraction beam to the CCD camera. The imaging lens's horizontal resolution (r_{lens}) is calibrated with the USAF horizontal resolution target. The actual resolution of the lens is in Fig. 3.

Group 5 of element 5 is the smallest distance distinguished by the lens, which corresponds to the lateral resolution of 9.84 μm . Hence, the verified experiment is conducted with two specific conditions: higher and lower lens resolution than grating groove spacing. The first setup uses the echelle grating with the groove spacing of 12.65 μm , which is lower than the lateral resolution of the imaging lens. The interference fringe image is captured after aligning the

optical path difference between two optical arms, as in Fig. 4(a). The interference image is subtracted to a background image to isolate the interference fringe and eliminate the background noise, as shown in Fig. 4(b). The full wide at half maxima (FWHM) of the fringe represents the axial resolution of the system, which is theoretically computed through the light source bandwidth ($\Delta\lambda$) and center wavelength (λ_c) as in (4).

$$\text{Axial resolution} = \frac{2\ln(2)\lambda_c^2}{\Delta\lambda} = 14.6 \mu\text{m} \quad (4)$$

The FWHM of the interference fringe is approximately 2.7 pixels by calibrating the camera pixel size, which corresponds to an axial resolution of 14.2 μm . The slight difference between experimental data and theoretical data is reasonable because the actual bandwidth of the customize comb light source is not steady as in the theoretical one.

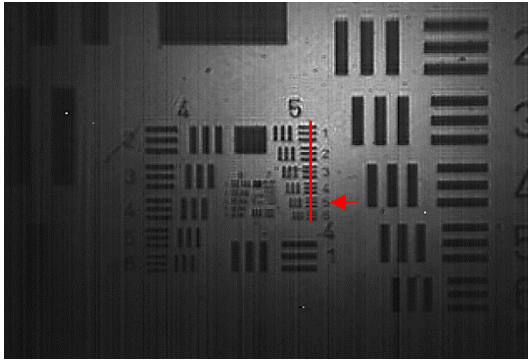


Fig. 3. Calibration of the lateral resolution of the imaging lens

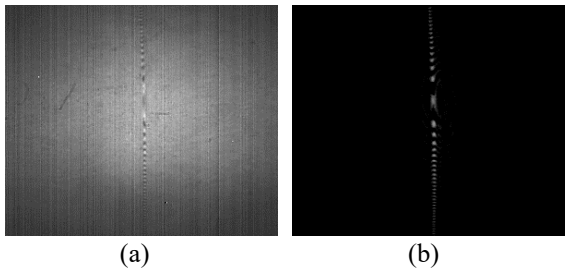


Fig. 4. The interference fringe images (a) raw image; (b) background-subtracted image

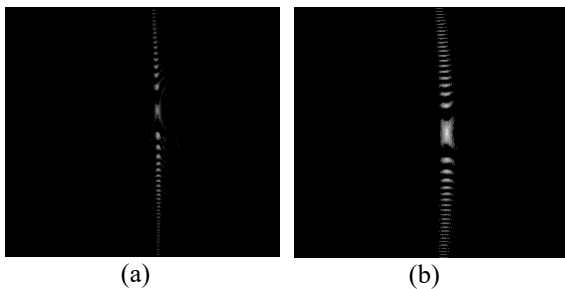


Fig. 5. The interference fringe images in (a) using the echelle grating; (b) blaze grating

The second experiment replaces the echelle grating with the blazed grating with the groove spacing of 3.33 μm , which is almost three times higher than the lateral resolution of the imaging lens. Fig. 5 compares the interference images in two cases. Fig. 5(a) shows interference fringe obtained using the echelle grating, which qualitatively shows a resolution higher than the fringe in Fig. 5(b) obtained by the blazed grating.

The quantitative calibration shows the agreement with the qualitative observation. The FWHM of the interference fringe obtained from the blazed grating is approximately 7 pixels, corresponding to an axial resolution of 24.3 μm . It shows that using the Echelle grating with the groove spacing lower than the lens resolution introduces a better axial resolution. Hence, the Echelle grating with groove spacing of 12.65 μm is selected to combine with an imaging lens with a focal length of 35 mm. The following experiment uses the selected components to measure a mirror displacement of 1 μm only, which previous results have not reached.

3.2. Measuring the 1 μm Mirror Displacement

The experimental setup is shown in Fig. 6 using the selected grating and imaging lens. The infrared optical pseudo comb with the bandwidth of 45nm and the center wavelength of 1290 nm introduces a sweep repetition rate of 29 kHz to overcome the flickering effect problem. The beam expander (2X) ensures the beam diameter fits the CCD camera size. A beam splitter with the R/T ratio of 30/70 is employed to balance the reflection intensity from two interference arms. A set of two spherical lenses (SLB1:35mm focal length, 30 mm diameter; SLB2: 100 mm focal length, 30 mm diameter) configured in 4f configuration is employed in the reference arm, while a set of a cylindrical lens (CLB: 100 mm focal length, 30 mm diameter) and a spherical lens (SLB: 35 mm focal length, 30 mm diameter) is employed in the sample arm. The CCD camera (FLIR Systems, Alpha NIR, InGaAs, 316x252pixels) with an exposure time of 100 μs is sufficient to capture the interference fringe without the vibration effect.

Consequently, an interference fringe appears on the screen, revealing the mirror position. Scanning the mirror along the optical axis leading the fringe scanned along the horizontal direction. A nanometer-resolution motor stage is integrated into the sample arm to ensure the precision of the mirror scanning with the displacement of 1 μm . The interference images at the first scanning position ($x = 0 \mu\text{m}$) and the second position ($x = 100 \mu\text{m}$) are recorded. The scanning process is repeated twenty-five times around two scanning positions to average the system's stability.

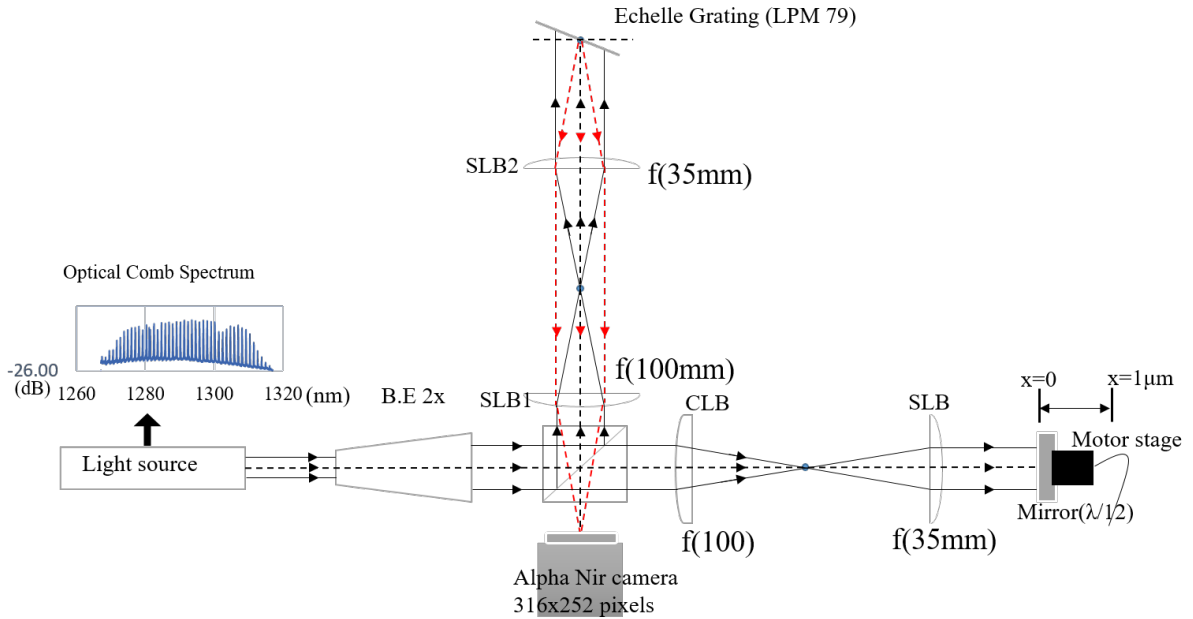


Fig. 6. Experimental setup of the proposed 2D single-shot comb-based interferometer

The following section determines the peak of interference fringes to reconstruct the mirror positions. The measurement accuracy and stability show the system's performance in the high-resolution inspection. Another experiment replaces the mirror sample with the Japanese 10-yen coin sample. The rough surface of the used coin challenges the typical interferometer using the visible laser source due to the high scattering effect. The proposed system is expected to overcome the scattering problem owing to the infrared light characteristic.

4. Experimental Results

4.1. Measuring the 1 μm Mirror Displacement

The experimental procedure consists of three main steps: capturing the interference image at two scanning positions, determining the interference fringe's peak position, and reconstructing the mirror positions. The measurement precision and stability are computed from the reconstructed positions to prove the system's ability to measure high-resolution displacement.

As mentioned, the twenty-five interference images are captured in each scanning position ($x = 0 \mu\text{m}$, and $x = 1 \mu\text{m}$) as in Fig. 7(a). The isolated interference fringe images are obtained by subtracting the raw images from a background image, respectively, in Fig. 7(b). The horizontal position of the subtracted images corresponds to the mirror scanning position. Hence, the precision of the fringe positions detection algorithm decides the precision of determining mirror positions.

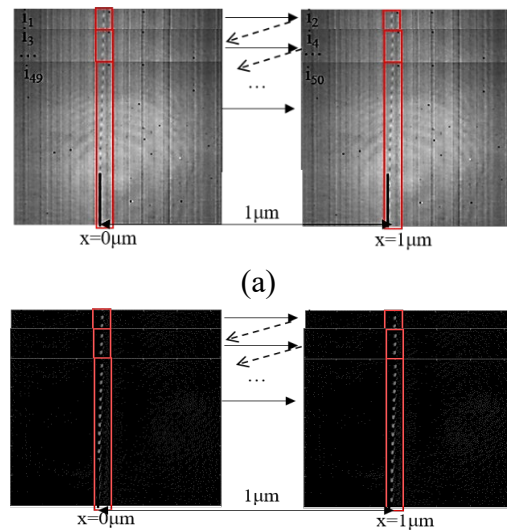


Fig. 7. Vertical scanning images (a) raw images; (b) subtracted images.

The region where the interference occurs in the image introduces the peak intensity compared to the background intensity. So, the Gaussian fitting algorithm is applied to fit the horizontal cross-section line of the fringe images into an envelope curve. The peak of the envelope curve represents the fringe position. Fig. 8(a) shows the horizontal cross-section of the first interference image (i_1) with the corresponding Gaussian fitting curve, shown in Fig. 8(b).

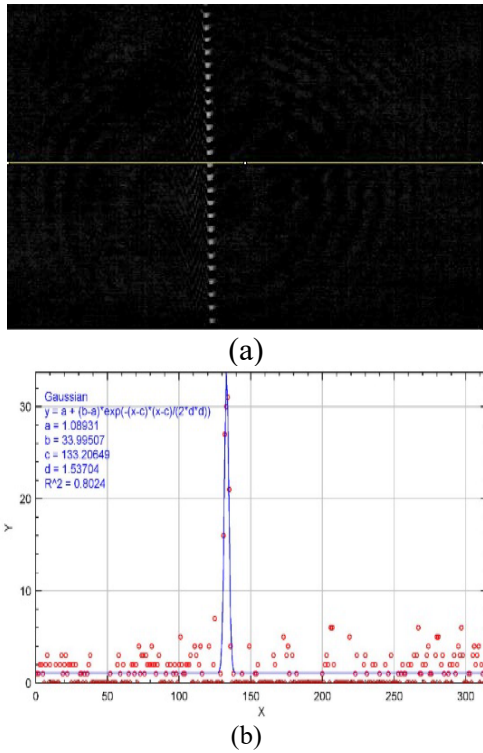


Fig. 8. (a) Horizontal cross-section of the interference image; (b) Gaussian fitting curve of the cross-section.

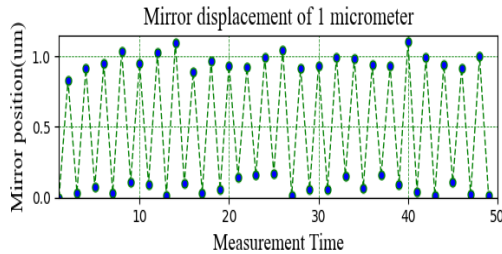


Fig. 9. The reconstructed mirror positions.

The constant value c corresponds to the horizontal position of the fringe at the pixel of 133.99. By calibrating the number of horizontal pixels (316 pixels) equivalent to the measurement range of the camera (1500 μm), the mirror position reconstructed from the first scanning image is 636.02 μm , used as an offset value. The reconstructed mirror positions are subtracted from the offset value to find the relative scanning positions of $x = 0 \mu\text{m}$ and $x = 1 \mu\text{m}$. Consequently, the relative mirror positions are reconstructed in Fig. 9.

The displacements of the mirror are computed by subtracting the two consecutive mirror positions. The average displacement is computed from twenty-five relative subtraction results by (5).

$$h_{\text{avg}} = \frac{|P2-P1|+|P3-P2|+\dots+|P50-P49|}{25} = 926.6(\text{nm}) \quad (5)$$

where $P1, P2, \dots, P100$ are the reconstructed mirror positions. While the stability of measurement is computed through the standard deviation

$$\text{std} = \sqrt{(h_{2-1}-h_{\text{avg}})^2 + (h_{3-2}-h_{\text{avg}})^2 + \dots + (h_{50-49}-h_{\text{avg}})^2} = 92.5(\text{nm})$$

The measurement accuracy of 92.7% with the stability of 92.5 nm is consistent, proving the proposed system's ability in a high-resolution measurement.

4.2. Measuring the Scattering Surface of a Japanese 10-Yen Coin

The system performance in measuring the scattering sample is also investigated. The interferometer measures a Japanese 10-yen coin with a high roughness surface, as in Fig. 10.

Three specific regions on the surface with different conditions are under inspection. The first region is a scattering background, the second region consists of three step-height blocks, and the third region contains the curve profile. The power of the light source increases from 350 μW to 700 μW to deal with the low reflection efficiency of the scattering surface.

The interference fringes can appear on the high roughness surface with an adequate high signal-to-noise ratio as in the raw images (a), (b), and (c) in Fig. 11. The fringe isolation images of (d), (e), and (f) are obtained after removing the background information. The form of the fringes corresponds to the profile of the coin surface. The first interference image shows a straight fringe of the surface background. The second image shows three step-height blocks with the separated distance, while the third image can perform the curve profile. From the obtained results, it is possible to reconstruct precisely the complete 3D profile of the coin with a pre-calibration of the camera pixel and a horizontal scanning process.



Fig. 10. The Japanese 10-yen coin

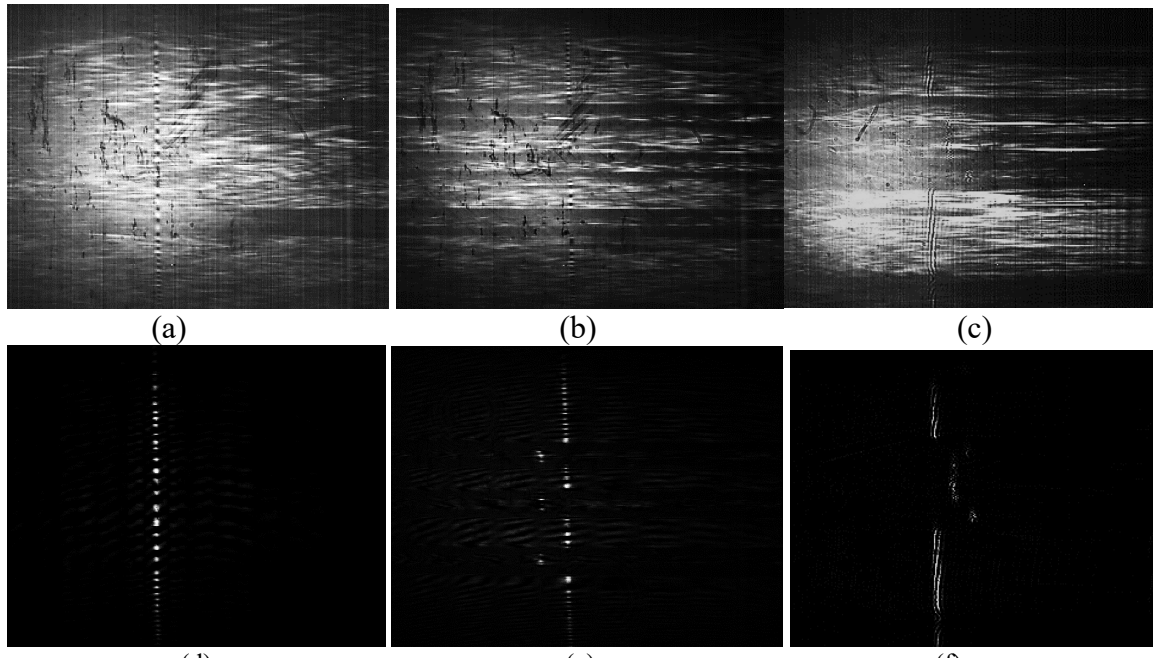


Fig. 11. Profilometry of the Japanese 10-yen coin

5. Discussion

The measurement results prove the system's ability in single-shot detection with high resolution. The accurate combination of the grating and imaging lens improves the measurement precision up to $1\ \mu\text{m}$, which was considered impossible in the previous setup. The resolution limitation can even extend to the sub-micrometer scale with upgrading devices discussed below.

5.1. Camera Pixel Size

The camera pixel size is $4.7\ \mu\text{m}/\text{pixel}$ obtained from the calibration process, significantly bigger than the measurement target of $1\ \mu\text{m}$ displacement. The sizable pixel causes the low precision of the curve fitting algorithm, limiting the system profilometry resolution, which is defined as the closest peak-to-peak distance detected from two Gaussian fitting curves of the interference fringe. The desired pixel size would be $0.2\ \mu\text{m}/\text{pixel}$, five times smaller than the measurement target.

5.2. Experimental Environment

It is noted that the optical system is not fixed in an optical isolation table. The air cushion system is turned off to challenge the system working in a vibration environment. Due to the high-speed single-shot detection, the vibration does not affect the fringe quality. However, the error in the scanning process might come from the movement error of the motor stage. Although the stage introduces the nanometer

scale movement, the lack of feedback loop decreases the relative translation precision.

5.3. Lens Aberration

The 4f lens system collects all the diffraction light from the sample to a corresponding pixel onto the CCD camera to remove the unwanted interference of the secondary point sources. It is also expected to cut off the spherical aberration. However, it is hard to eliminate the aberration from the broadband light. The achromatic and spherical deformation still occurs, causing the deformed interference fringe.

6. Conclusion

The 2D single-shot comb-based interferometer proved to be a powerful tool for industrial inline inspection due to the high-speed detection, high resolution, and flexible long-range measurement. The research provides deep analysis to optimize the measurement precision of the system. The effect of the critical components in the reference module is investigated. The system with selected components improves the measurement precision significantly to reach the sub-micrometer resolution. The experimental result also mentions the system's ability to measure the scattering surface, which is the challenge of the typical interferometers using visible light. The research opens the system's various opportunities to broaden the measurement sample in the industrial inline inspection.

References

- [1] Smith F H, Microscopic interferometry, Research (London) (1955) 152-160.
- [2] D. Huang, E.A. Swanson, C.P. Lin, J.S. Schuman, W.G. Stinson, W. Chang, M.R.Hee, T. Flotte, K. Gregory, C.A. Puliafito, J.G. Fujimoto, Optical coherence tomography, *Sci.* 254 (1991) 1178
<https://doi.org/10.1126/science.1957169>
- [3] Leslie Deck, Peter de Groot, High-speed noncontact profiler based on scanning white-light interferometry, *Appl.Opt.*33 (31) (1994).
<https://doi.org/10.1364/AO.33.007334>
- [4] R. Leitgeb, M. Wojtkowski, A. Kowalczyk, C. K. Hitzenberger, M. Sticker, and A. F. Fercher, Spectral measurement of absorption by spectroscopic frequency-domain optical coherence tomography, *Opt. Lett.*25 (2000) 820.
<https://doi.org/10.1364/OL.25.000820>
- [5] Samuel Choi, Mitsufumi Yamamoto, Daisuke Moteki, Tatsutoshi Shioda, Yosuke Tanaka, and Takashi Kurokawa, Frequency-comb-based interferometer for profilometry and tomography, *Opt. Lett.*31 (2006).
<https://doi.org/10.1364/OL.31.001976>
- [6] T. Shioda, T. Morisaki, and H. Ono, Single-shot tomography by means of VIPA and spatial phase modulator installed optical interferometer, *Opt. Commun.* 284, 144–147.
<https://doi.org/10.1016/j.optcom.2010.09.028>
- [7] Tuan Quoc Banh, Kohei Suzuki, Munehiro Kimura, and Tatsutoshi Shioda, Two-dimensional high-speed and long-range tomography and profilometry using liquid-crystal Fabry–Perot resonator, *Appl. Opt.* 54, 912 (2015).
<https://doi.org/10.1364/AO.54.000912>
- [8] Tuan Cong Truong, Tuan Quoc Banh, Heuihyeon Kim, Tatsutoshi Shioda, Axial zoomable 2D single-shot comb interferometry using spatial phase modulator for profilometry and tomography, *Opt. Commun.* 439, (2019), 276-283.
<https://doi.org/10.1016/j.optcom.2019.01.029>
- [9] Tuan Cong Truong, Tuan Quoc Banh, Tatsutoshi Shioda, Development of discrete frequency swept laser for 2D single-shot pseudo comb interferometry, *Jpn. J. Appl. Phys.* 58 056503 (2019).
<https://doi.org/10.7567/1347-4065/ab0a7f>